Quantitative SNR Analysis for ISAR Imaging Using Joint Time-Frequency Analysis—Short Time Fourier Transform

V. C. Chen recently presented an inverse synthetic aperture radar (ISAR) imaging technique using the joint time-frequency analysis (JTFA), which has been shown having a better performance for maneuvering targets over the conventional Fourier transform method. The main reason is because the frequencies of the radar returns of the maneuvering targets are time varying and a JTFA is a technique that is suitable for such signals, in particular a JTFA may concentrate a wideband signal, such as a chirp, while it spreads noise. We quantitatively study the signal-to-noise ratio (SNR) in the ISAR imaging using one of the typical JTFA techniques, namely the short time Fourier transform (STFT). We show that the SNR increases in the joint time-frequency (TF) domain over the one in the time or the frequency domain alone both theoretically and numerically. This quantitatively shows the advantage of the JTFA technique for the ISAR imaging.

I. INTRODUCTION

To obtain a high resolution inverse synthetic aperture radar (ISAR) imaging in the range direction, the radar transmits a wideband signal (such as linear frequency modulated (LFM) or stepped-frequency waveform). The high resolution in the cross-range direction is obtained by using the Doppler information of the returned signal. Due to the object's rotation, different parts of the object have different velocities relative to the stationary radar, which are detected as the Doppler information and used to form the image of the object. The conventional method for the Doppler shift detection is the Fourier transform, which is effective only for stationary frequencies, i.e., constant speed rotations of a rotating object. In many circumstances, the rotation speeds are time varying. In this case, the Fourier transform can not accumulate the signal of a scatterer but transforms it to a signal in a wide band, which causes the image of the target smeared. Based on this observation, Chen,

et al. [1–5] proposed a new ISAR imaging technique using joint time-frequency analysis (JTFA) which may accumulate some radar return signals of a scatterer with time-varying frequencies, such as chirps, in the joint time-frequency (TF) plane. Significant ISAR imaging performance improvement has been shown in [1–5], where, however, no quantitative analysis is provided.

It is known that a JTFA maps one-dimensional signals in the time domain into two-dimensional signals in both the time and the frequency domains, see for example [11–12]. Unlike the traditional Fourier transform that only concentrates narrowband signals, a JTFA also *concentrates* some wideband signals, such as chirps. In the meantime, similar to the Fourier transform that *spreads* the noise from the time domain into the frequency domain, a JTFA *spreads* the noise from the time domain into the joint time and frequency domain. The goal of this work is two-fold. First, we study the signal-to-noise ratio (SNR) for the short time Fourier transform (STFT), one of the most important JTFAs, for analog signals and calculate the SNR in the STFT domain in terms of the new definition in [6] for linear chirp signals. Note that the SNR results obtained in [6] are for discrete signals. We find the connection between the SNR for the STFT of analog signals and the one of discrete signals. It is shown that the SNR in the JTFA domain increases over the one in either the time or the frequency domain. Second, we apply the SNR analysis to the ISAR imaging proposed by Chen, et al. [1–5] when the STFT is used. One can not only see that the SNR increases in the ISAR image but also see that the ISAR image improves over the conventional Fourier transform technique due to the increase of the signal mean power in the joint TF domain.

This paper is organized as follows. In Section II, we formulate the radar return signal model after the range compression and motion compensation but before the Doppler processing and then briefly review the ISAR imaging method proposed by Chen, et al. [1–5]. In Section III, we describe the SNR analysis for the STFT and apply it to the ISAR imaging. In Section IV, we present some simulation results to show the SNR increase.

II. ISAR IMAGING OF MANEUVERING TARGETS

In this section, we briefly review ISAR imaging algorithms for maneuvering targets.

In ISAR imaging, the radar is stationary and transmits wideband electromagnetic waves to a moving target. The high resolution can be obtained in the range direction for the high wideband transmitted signal. After the range compression and the motion compensation to the received signal, the returned signal of scatterer P can be finally written as, see for

example [1–5],

$$s(t) = \frac{A_P}{\sqrt{T}}\text{rect}\left(\frac{t}{T}\right)\exp\left(j\left(\omega_{0,P}t + \frac{\omega_{1,P}}{2}t^2\right)\right) \quad (1)$$

where A_P is the refectivity of scatterer P, T is the coherent integration time of imaging (slow time interval length), $\omega_{0,P}$ and $\omega_{1,P}$ are the frequency and the frequency rate of the signal, respectively, which depends on the target motion with respect to radar and the position of the scatterer in the target. The polar format processing is needed, if target size or the target rotating angle with respect to the line of radar sight is large [16]. When there is an additive noise, the returned signal is

$$\tilde{s}(t) = s(t) + n(t). \quad (2)$$

When there are K scatterers in a range, the received signal of a range bin after the motion compensation is

$$\tilde{s}(t) = \sum_{i=1}^{K} s_i(t) + n(t) \quad (3)$$

where $s_i(t)$ are LFM signals that have the same form as $s(t)$ in (1) but different parameters ω_0 and ω_1. In conclusion, the returned signal of the radar transmission before the Doppler processing is a linear combination of LFM signals, which is not because the transmitted signal is an LFM but because of the rotation of the target. For detailed derivations, see for example [14–16].

The conventional ISAR imaging method is to take the Fourier transform to each range cell's signal after the range compression and motion compensation, i.e., take the Fourier transform of $\tilde{s}(t)$ in (3).

The Fourier transform of $s(t)$ is

$$M(f) = \frac{A_P}{\sqrt{2|k|T}}$$
$$\times \exp(-j\pi f^2(C(Z_1) + C(Z_2) \pm j(S(Z_1) + S(Z_2)))) \quad (4)$$

where $Z_1 = \sqrt{2|k|}(T/2 - f/k)$, $Z_2 = \sqrt{2|k|}(T/2 + f/k)$, $C(Z) = \int_0^z \cos(\pi/2\xi^2)d\xi$, and $S(Z) = \int_0^z \sin(\pi/2\xi^2)d\xi$, see for example [13]. Let B be the frequency deviation as $B = \Delta f = \omega_1 T/2\pi$. When B is not small, the received signal has its Fourier spectrum with full band. In this case, the SNR_f of the Fourier transform technique of the signal is in the order of the one, SNR_t, in the time domain.

As mentioned in the Introduction, the conventional Fourier transform does not provide a satisfactory performance for accumulating such a signal s_i for the ith scatterer in the frequency domain while the JTFA does in the joint TF plane. By replacing the Fourier transform with a JTFA in the Doppler processing, the ISAR imaging method proposed by Chen, et al. [1–5] can be described in Fig. 1, where instead of a single

image there are a sequence of images that form an ISAR image cube.

JTFA is a class of transformations, which includes STFT, Wigner-Ville distributions (WVD), and adaptive chirplet transform (ACT), etc. The basic idea using JTFA in ISAR imaging is to first decompose the received signal $\tilde{s}(t)$ in (3) into several subsignals $s_m(t)$, $m = 1,\ldots,M$, each of which has some particualar properties (subsignal has sinusoid-like property to STFT, and chirp-like property to ACT). Then, WVD $\text{WVD}_{s_m}(t,\omega)$ is taken to each of the subsignal $s_m(t)$, $m = 1,\ldots,M$, since WVD is optimal (in terms of the concentration) for a single component signal [10–12]. Next, all the WVDs $\text{WVD}_{s_m}(t,\omega)$ are added to get a TF distribution $\text{TFD}_{\tilde{s}}(t,\omega) = \sum_{m=1}^{M} \text{WVD}_{s_m}(t,\omega)$ of the signal $\tilde{s}(t)$. Therefore, there is no cross terms among subsignals in the TF distribution $\text{TFD}_{\tilde{s}}(t,\omega)$. At last, the amplitude and instantaneous frequency of each scatterer are obtained at a time instant t_0 from $\text{TFD}_{\tilde{s}}(t_0,\omega)$ to form the image.

In the next section, we analyze the SNR for the ISAR image formed in Fig. 1 when the STFT is used.

III. SNR FOR ISAR IMAGING USING JTFA

In this section, we focus on the signal model before the Doppler processing, which is given in (1)–(3). We first give the new SNR definition and then calculate the SNR for the STFT for both analog and discrete LFM signals in (3).

A. New SNR Definition

As mentioned in the Introduction, the conventional SNR is defined as the ratio of the mean power of the signal over the mean power of the noise, where the mean is taken over the whole domain. It is formulated as follows. Let $y[n]$ be a distorted signal:

$$y[n] = x[n] + \eta[n], \qquad 0 \le n \le N - 1 \quad (5)$$

where the variable n is in a domain, such as the time domain, the frequency domain, etc., $x[n]$ is a signal and $\eta[n]$ is an additive noise with mean zero and variance σ^2. The SNR is defined as

$$\text{SNR} = \frac{\sum_{n=0}^{N-1} |x[n]|^2}{N\sigma^2}. \quad (6)$$

Clearly any energy preserving transformation does not change the above SNR, which is not appropriate for some signals, such as narrowband signals in the Fourier transform domain and chirps in the joint time-frequency transformation domain. A common characteristic of such signals is that they are not stationary in the transform domain and therefore the average taking over the whole domain is not proper. A new definition was given in [6], which is stated as follows.
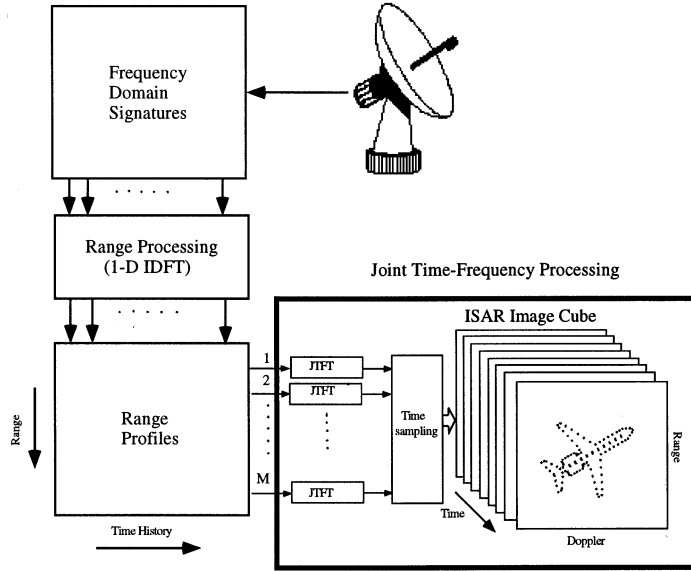
Fig. 1. ISAR imaging using JTFA.

DEFINITION 1 For the signal $x[n]$ of length N, $0 \leq n \leq N - 1$, let

$$\mathcal{B} \stackrel{\Delta}{=} = \left\{ n : 0 \leq n \leq N - 1 \qquad \text{and} \right.$$

$$\left. |x[n]|^2 \geq 0.5 \max_{0 \leq n \leq N-1} |x[n]|^2 \right\} \qquad (7)$$

where the number 0.5 comes from the common 3 dB bandwidth definition in communications. Then, the SNR is defined as

$$\text{SNR} \stackrel{\Delta}{=} \frac{\sum_{n \in \mathcal{B}} |x[n]|^2}{|\mathcal{B}| \sigma^2} \qquad (8)$$

where $|\mathcal{B}|$ denotes the cardinality of the set $\mathcal{B}$.

The SNR for analog signals can be similarly defined. Notice that this definition is similar to the SNR definition in communications, where the signal is only considered in its bandwidth. Also the SNR using the ratio of the peak squared magnitude over the mean noise power is used in some literature, which may not be valid if the signal contains more than the peak value, such as the curves in the TF domain. Examples shown in [6] have illustrated the better indication of signal and noise levels in various domains. In what follows, we adopt the above new SNR definition.

B. SNR for STFT and ISAR Imaging

We first consider the STFT for analog LFM signals in (3). For convenience, let us first consider single LFM $s(t)$ in (1)–(2), i.e.,

$$\tilde{s}(t) = s(t) + n(t) = A \exp\left(-j\left(\omega_0 t + \frac{\omega_1}{2} t^2\right)\right) + n(t)$$

$$-\frac{T}{2} \leq t \leq \frac{T}{2} \qquad (9)$$

where A is the signal amplitude, and $n(t)$ is the additive white noise with the following correlation function

$$R_n(t, s) = E(n(t)n^*(s)) = \sigma^2 \delta(t - s)$$

$$-\frac{T}{2} \leq t, \quad s \leq \frac{T}{2}. \qquad (10)$$

Consider the STFT with the Gaussian window function

$$g_\alpha(t) = \left(\frac{\alpha}{\pi}\right)^{1/4} \exp\left(-\frac{\alpha}{2} t^2\right), \qquad \alpha > 0 \qquad (11)$$

where α is a parameter. Notice that the above Gaussian window function is optimal in terms of the TF localization from the uncertainty principle, see for example, [11]. The STFT of a signal $x(t)$ is

$$\text{STFT}_x(t, \omega) = \int_{-\infty}^{\infty} x(s) g_\alpha(s - t) \exp(-js\omega) ds \qquad (12)$$

where $x(t)$ can be either $s(t)$ or $n(t)$ in this context. Thus, see for example [11, 12],

$$|\text{STFT}_x(t, \omega)|^2 = \iint \text{WVD}_x(u, v)$$

$$\cdot \text{WVD}_{g_\alpha}(t - u, \omega - v) du \, dv \qquad (13)$$

where WVD stands for the Wigner-Ville distribution. Since the STFT is a linear transformation, we consider the STFT for the signal $s(t)$ and the noise $n(t)$ separately.

It is not hard to see that the WVD of the above $s(t)$ is

$$\text{WVD}_s(t, \omega) = A^2 T \operatorname{sinc}\left[\frac{(\pi\omega - \omega_1 t - \omega_0)T}{\pi(\omega - \omega_1 t - \omega_0)T}\right].$$

$$(14)$$

CORRESPONDENCE

651

Since an ISAR target is usually small, the angle that a target rotates in the imaging is small (about $1°$–$3°$) while the imaging time T is usually not too small, (14) can be approximated as

$$\text{WVD}_s(t,\omega) \approx A^2 \delta(\omega - \omega_1 t - \omega_0). \qquad (15)$$

The WVD of the window function is, see for example [11–12],

$$\text{WVD}_{g_\alpha}(t,\omega) = 2\exp\left(-\left(\alpha t^2 + \frac{1}{\alpha}\omega^2\right)\right). \qquad (16)$$

Thus, the STFT of the signal is

$$|\text{STFT}_s(t,\omega)|^2 = 2A^2 \iint \delta(v - \omega_1 u - \omega_0)$$

$$\times \exp\left(-\left(\alpha(t-u)^2 + \frac{1}{\alpha}(\omega-v)^2\right)\right)du\,dv$$

$$= \frac{2A^2\sqrt{2\pi}}{\sqrt{2\left(\alpha + \frac{1}{\alpha}\omega_1^2\right)}}\exp\left(-\frac{(\omega - t\omega_1 - \omega_0)^2}{\alpha + \frac{1}{\alpha}\omega_1^2}\right). \tag{17}$$

In this case, the maximum of $|\text{STFT}_s(t,\omega)|^2$ is reached when $\omega = t\omega_1 + \omega_0$ and the maximum is

$$\max_{t,\omega}|\text{STFT}_s(t,\omega)|^2 = \frac{2A^2\sqrt{\pi}}{\sqrt{\alpha + \frac{1}{\alpha}\omega_1^2}}. \qquad (18)$$

Therefore, the 3 dB mean of $|\text{STFT}_s(t,\omega)|^2$ in the new SNR definition (7)–(8) is

$$\text{mean}_{(t,\omega)\in\mathcal{S}}|\text{STFT}_s(t,\omega)|^2 \qquad (19)$$

where

$$\mathcal{S} = \left\{(t,\omega) : |\text{STFT}_s(t,\omega)|^2 > 0.5\frac{2A^2\sqrt{\pi}}{\sqrt{\alpha + \frac{1}{\alpha}\omega_1^2}}\right\}. \qquad (20)$$

Clearly, using (17)

$$\mathcal{S} = \left\{|\omega - t\omega_1 - \omega_0|^2 < \left(\alpha + \frac{1}{\alpha}\omega_1^2\right)\ln 2\right\}.$$

Thus, the 3 dB mean signal power is

$$\text{mean}_{(t,\omega)\in\mathcal{S}}|\text{STFT}_s(t,\omega)|^2$$

$$= \frac{2A^2\sqrt{\pi}}{\sqrt{\alpha + \frac{1}{\alpha}\omega_1^2}}\frac{1}{\sqrt{\ln 2}}\int_0^{\sqrt{\ln 2}}\exp(-u^2)\,du. \qquad (21)$$

After the 3 dB mean signal power is calculated, let us calculate the mean noise power. Since the noise $n(t)$ is stationary, its mean power can be calculated in the sample space as follows. Using (10) we have

$$E|\text{STFT}_n(t,\omega)|^2 = E\left|\int_{-\infty}^{\infty} n(s)g_\alpha(s-t)\exp(-js\omega)\,ds\right|^2$$

$$= \sigma^2 \int |g_\alpha(s)|^2\,ds = \sigma^2. \qquad (22)$$

Therefore, by (21)–(22) the SNR in the STFT domain is

$$\text{SNR}_{tf} = \frac{2a\sqrt{\pi}A^2}{\sqrt{\alpha + \frac{1}{\alpha}\omega_1^2}\sigma^2} = \frac{2a\sqrt{\pi}}{\sqrt{\alpha + \frac{1}{\alpha}\omega_1^2}}\text{SNR}_t \qquad (23)$$

where $\text{SNR}_t = A^2/\sigma^2$ is the SNR in the time domain (which is equal to the conventional SNR), and

$$a = \frac{1}{\sqrt{\ln 2}}\int_0^{\sqrt{\ln 2}}\exp(-u^2)\,du \approx 0.8. \qquad (24)$$

The maximum of the SNR_{tf} in terms of the parameter α in the STFT window function $g_\alpha(t)$ in (11) is reached when

$$\alpha = |\omega_1| \qquad (25)$$

and the maximum is

$$\text{SNR}_{tf}^{\max} = \max_\alpha \text{SNR}_{tf} = 0.8\frac{\sqrt{2\pi}}{\sqrt{|\omega_1|}}\cdot\text{SNR}_t. \qquad (26)$$

For the multiple LFM signal model (3) with K components with the same mean power, the maximum of the SNR_{tf} in terms of α is bounded by

$$0.8\frac{\sqrt{2\pi}}{\sqrt{\max_{1\le i\le K}|\omega_i|}}\cdot\text{SNR}_t \le \text{SNR}_{tf}^{\max} = \max_\alpha\text{SNR}_{tf}$$

$$\le 0.8\frac{\sqrt{2\pi}}{\sqrt{\min_{1\le i\le K}|\omega_i|}}\cdot\text{SNR}_t \qquad (27)$$

i.e., it is between the maximum and the minimum of the components in (26). Clearly,

$$\text{when}\quad \max_{1\le i\le K}|\omega_i| < 1.28\pi,$$
$$\text{we have}\quad \text{SNR}_{tf}^{\max} > \text{SNR}_t \qquad (28)$$

i.e., the SNR in the STFT domain is greater than the SNR in the time domain. The SNR formulas in (28) also imply that, when the absolute values of the coefficients, i.e., the accelerations of the scatterers, ω_i in the LFM $s_i(t)$ are not too large, the SNR in the STFT domain is greater than the one in the time domain.

It is known that, when the coefficients ω_i in the LFM $s_i(t)$ are small, the bandwidth of $s(t)$ may not
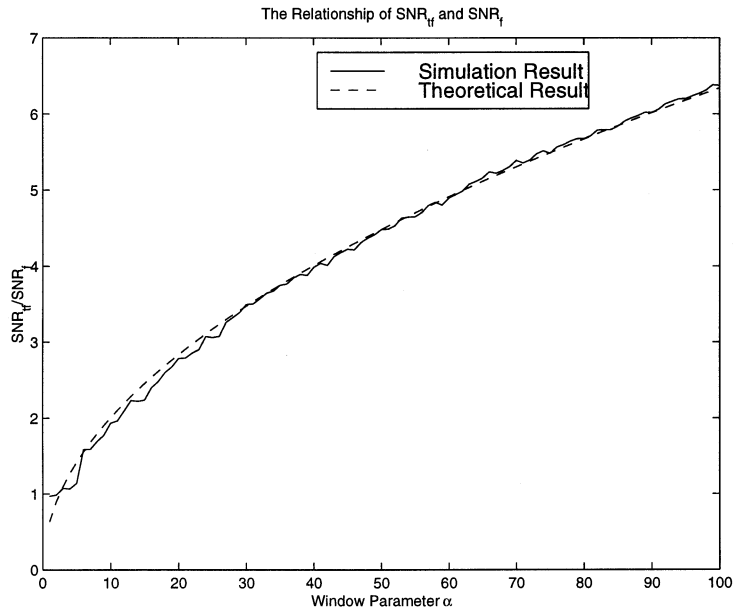
The Relationship of SNR$_{tf}$ and SNR$_f$

Fig. 2. Relationship of SNR$_f$ and SNR$_{tf}$ with optimal wndow parameter.
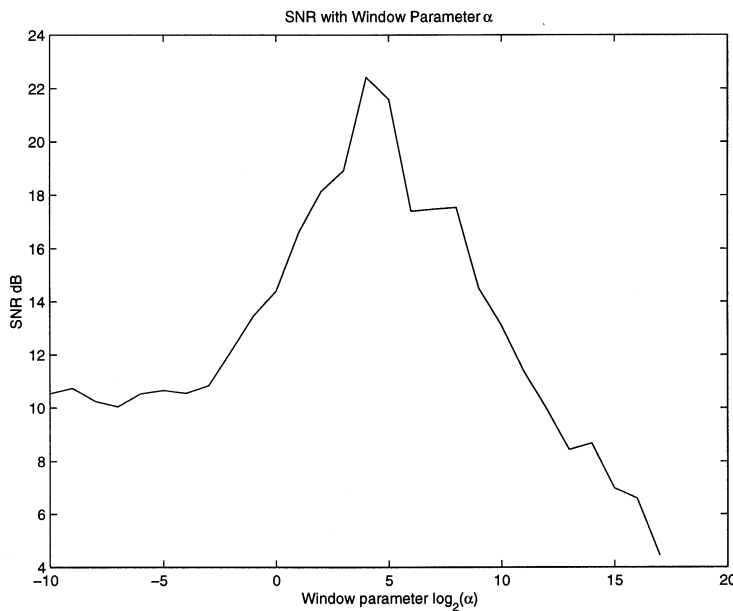

SNR with Window Parameter α

Fig. 3. Relationship of SNR$_{tf}$ with window parameter α. Peak is reached when $\alpha = 16$.

be large. In other words, the 3 dB SNR, SNR$_f$, in the Fourier transform domain may be also greater than the one in the time domain. This raises the question: which SNR of SNR$_{tf}$ and SNR$_f$ is better? We next want to compare these two SNRs in the STFT domain and in the Fourier transform domain. If the time-bandwith product $TB = \omega T^2$ is larger, $s(t)$ has approximately a constant-amplitude spectrum in $\omega_0 - (B/2) \leq f \leq \omega_0 + (B/2)$. If the time-bandwith product BT is not large enough the spectrum of $s(t)$ is spread out of the band $\omega_0 - (B/2) \leq f \leq \omega_0 + (B/2)$ with high sidelobes. The 3 dB mean power of the Fourier transform $S_i(f)$ of $s_i(t)$ is, thus, less than or

equal to

$$\frac{\text{Energy of } S_i}{B_i}$$

where B_i is the bandwidth of the s_i, i.e., $B_i = |\omega_i| T$, see for example [13]. Since the Fourier transform preserves the signal energy, the 3 dB SNR in the Fourier transform of $s_i(t)$ is, thus,

$$\text{SNR}_f \leq \frac{T A^2}{B_i \sigma^2}$$

where A^2 is the power of s_i in (1). This provides the SNR in the frequency domain for the LFM s_i:

$$\text{SNR}_f \leq \frac{1}{|\omega_i|} \cdot \text{SNR}_t.$$
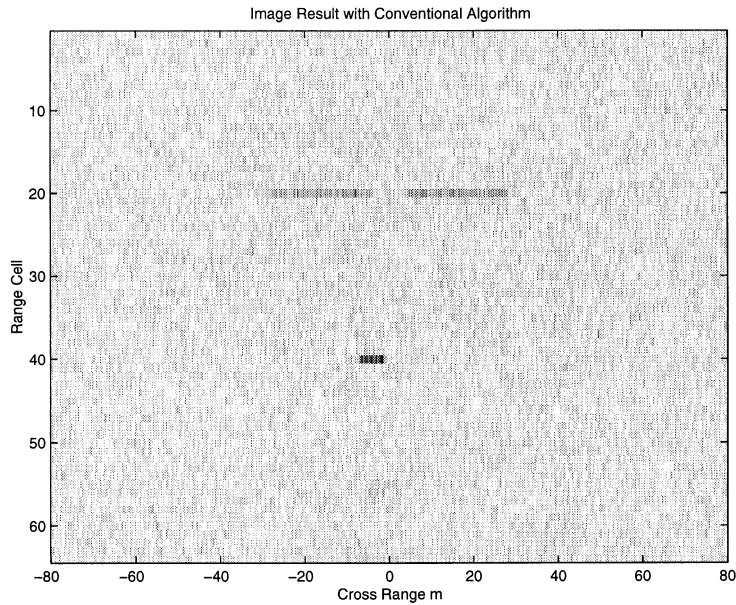
CORRESPONDENCE

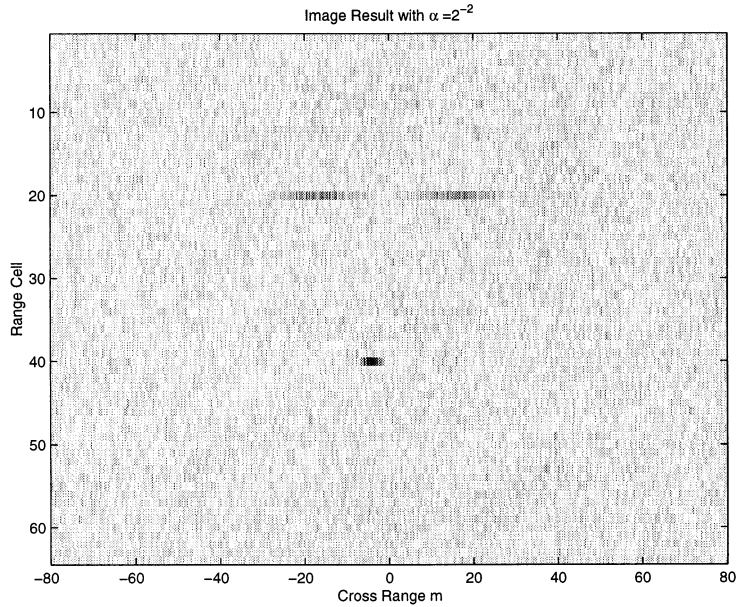653

Fig. 4.   Imaging result with conventional algorithm.

Fig. 5.   Imaging result with $\alpha = 2^{-2}$.

Therefore, we have

$$\mathrm{SNR}_{tf}^{\max} = \frac{0.8\sqrt{2\pi}}{\sqrt{|\omega_i|}} \cdot \mathrm{SNR}_t \geq 0.8\sqrt{2\pi}\sqrt{|\omega_i|} \cdot \mathrm{SNR}_f$$

$$(29)$$

i.e.,

$$\frac{\mathrm{SNR}_{tf}^{\max}}{\mathrm{SNR}_f} \geq 0.8\sqrt{2\pi}\sqrt{|\omega_i|}. \qquad (30)$$

This result implies that, when

$$|\omega_i| > 1/(0.8\sqrt{2\pi})^2 = 0.2487 \qquad (31)$$

we have

$$\mathrm{SNR}_{tf}^{\max} > \mathrm{SNR}_f.$$

Similar argument applies to the SNR in the frequency domain for LFM combination $s(t)$ in (3) by considering the maximum coefficient $\max_{1 \leq i \leq K} |\omega_i|$. In conclusion, we have analytically shown that the SNR of the STFT for LFM is also better than the one of the Fourier transform when the chirp rate is not too small, which will be also seen from the numerical simulations presented in the next section.

All the above analysis is for analog LFM signals, where the sampling rate is not concerned. In practical calculations, the analog signals need to be sampled and thus the sampling rate plays an important role. The SNR analysis for the discrete STFT, i.e., the STFT for discrete time signals and
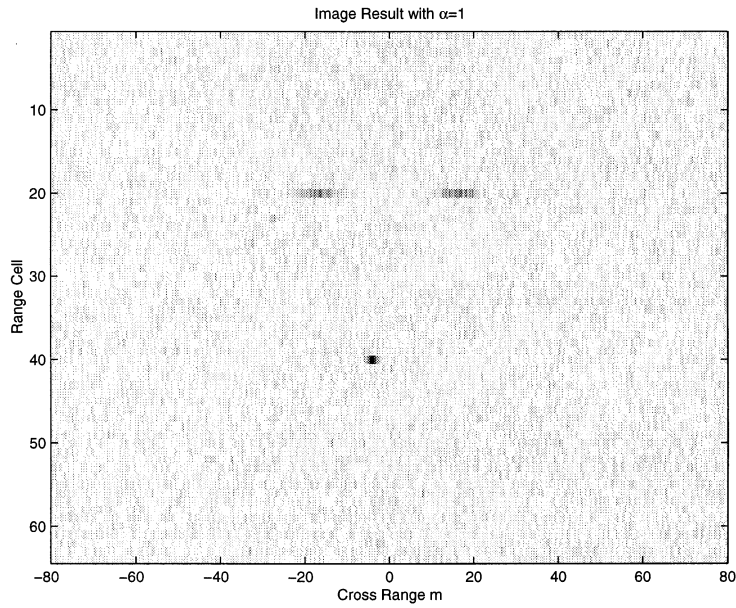
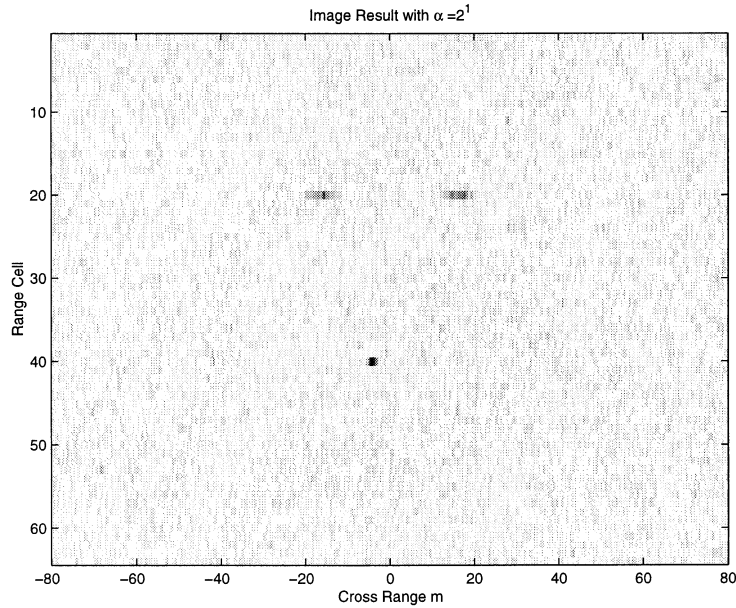Fig. 6. Imaging result with $\alpha = 1$.

Fig. 7. Imaging result with $\alpha = 2^1$.

rectangular window functions, was recently obtained in [6] in terms of the sampling rate. It can be stated as follows. For a multicomponent signal with K monocomponents, the SNR in the discrete STFT domain is

$$\text{SNR}_{tf}^{\text{discrete}} \approx D \frac{N}{K} \cdot \text{SNR}_t \qquad (32)$$

where D is a constant, N/T_0 is the sampling rate, and T_0 is the window length in the discrete STFT. We next discuss a relationship between the SNR, the coefficient $|\omega_i|$, the sampling rate, and the STFT window length.

For simplicity, we consider the following sampled signal

$$s_T \left(\frac{k}{N} \right) = \exp(j\omega_1 (T_0 k/N)^2),$$

$$k = 0, 1, \ldots, N - 1 \qquad (33)$$

where N is the sampling rate and T_0 is the STFT window length. We now have the following two cases.

Case 1   Let the coefficient ω_1 fixed. In this case, the sampling rate N goes to infinity is *equivalent* to the window length T_0 goes to zero by absorbing $1/N$ into T_0 in (33).
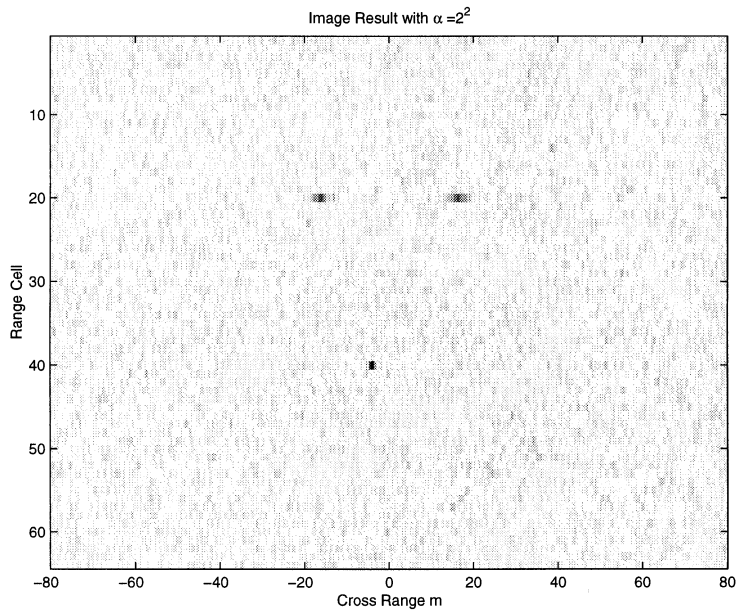
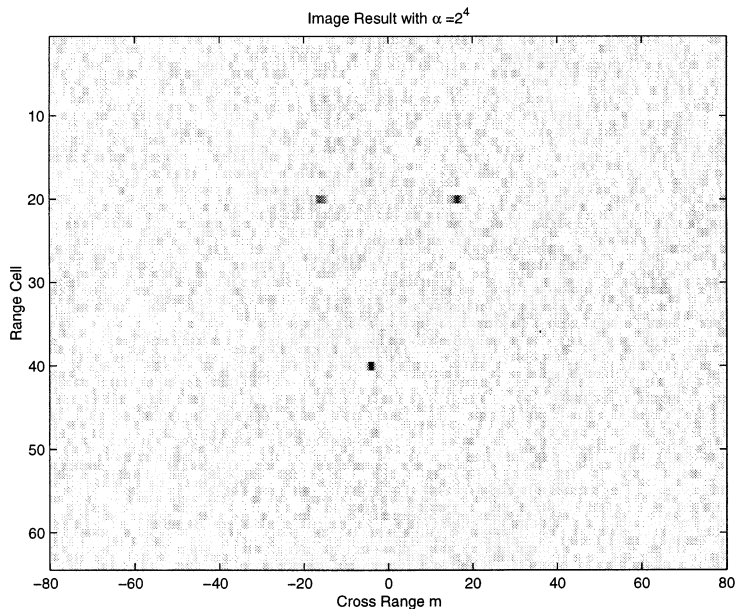CORRESPONDENCE

Fig. 8. Imaging result with $\alpha = 2^2$.

Fig. 9. Imaging result with $\alpha = 2^4$.

Case 2 Let the sampling rate N fixed. In this case, the window length T_0 goes to zero is *equivalent* to the coefficient ω_1 goes to zero by absorbing T_0^2 into ω_1 in (33).

From the SNR analysis of the discrete STFT for discrete time signals, the SNR in the STFT domain goes to infinity, (32), when the sampling rate goes to infinity. From the SNR analysis of the STFT for analog signals, the SNR in the STFT domain goes to infinity, (26), when the coefficient ω_1 goes to zero. From the above Cases 1 and 2, these two results are equivalent, i.e., (32) is equivalent to (26), from the SNR increase perspective.

All the above SNR analyses apply to the ISAR imaging in Fig. 1 proposed by Chen, et al. [1–5] when the STFT is used as the JTFA. Notice that the JTFA in the ISAR imaging proposed in [1–5] is not limited to a particular one. A similar SNR increase for using other JTFA rather than the STFT is also expected due to the fact that the STFT usually has lower resolution than other JTFA, such as WVD, do.

Another point we want to make here is that the above SNR increase in the STFT domain is due to the mean signal power increase. It is because the JTFA concentrates the LFM signals better than the Fourier transform does. This property also indicates that the better ISAR imaging quality using the JTFA can be
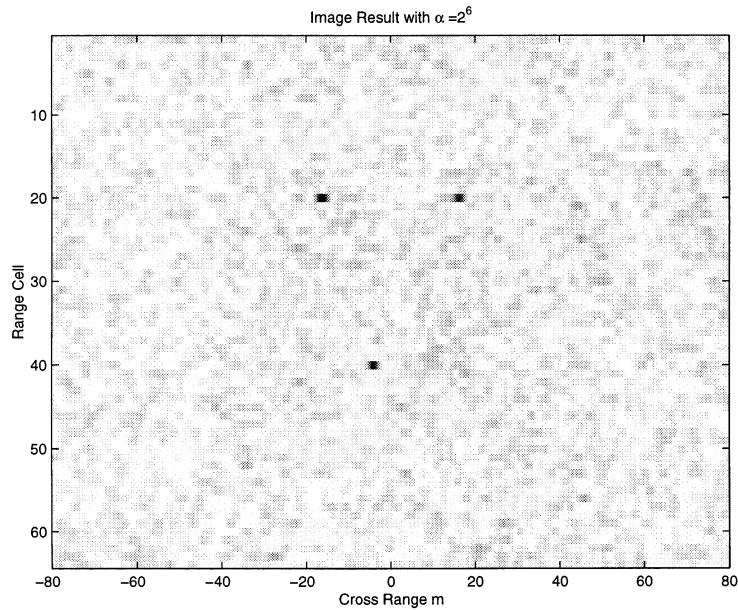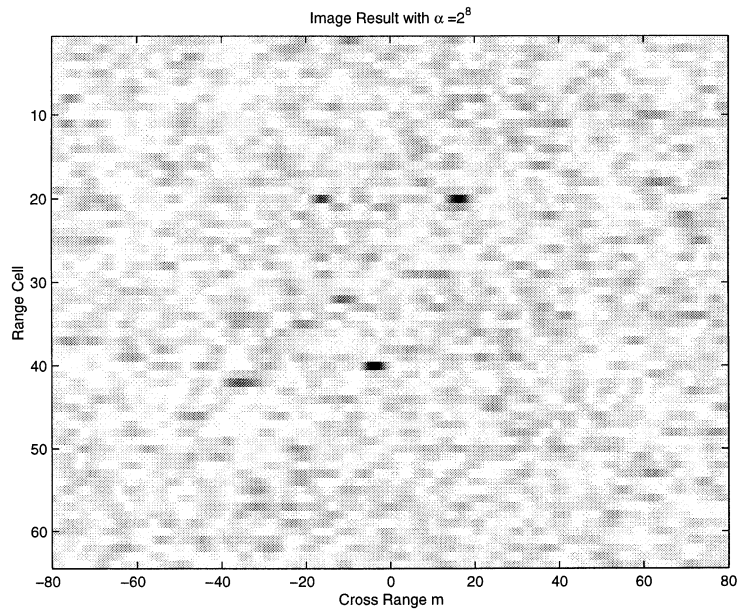
Fig. 10. Imaging result with $\alpha = 2^6$.

Fig. 11. Imaging result with $\alpha = 2^8$.

achieved over the one using the Fourier transform, which is seen from the simulation results in the next section.

IV. SIMULATION RESULTS

Let us present some simulation results. First, the relationship between SNR_f and SNR_{tf} with the optimal window parameter α is shown in Fig. 2. It is shown that the larger the chirp rate of a signal is, the larger the SNR can be obtained by using the STFT than by using the Fourier transform. In the simulation, signal $s(t) = \exp\{j(\omega_0 t + (\omega_1/2)t^2)\}$ is used. For a given chirp rate ω_1, the result in the Fig. 2 is obtained by averaging the results with different ω_0 as $\omega_0 = 5$, 10, 15, 20, 25, 30, 35, 40, 45, 50. The simulation result (solid curve) matches the theoretical result (30) (dashed curve). Then, the relationship between SNR_{tf} and the window parameter α is shown in Fig. 3. In this simulation, signal $s(t) = \exp\{-j(2t + 8t^2)\} + n(t)$ is used, where time t varies from -3 s to 3 s with sampling rate 333 Hz and signal energy to noise energy ratio -3 dB. From this simulation result, we can find that the 3 dB SNR_{tf} in the TF domain reaches the highest value when the window parameter α matches the signal chirp rate.

We next present some ISAR imaging results (given from Figs. 4–13) by using the Fourier transform
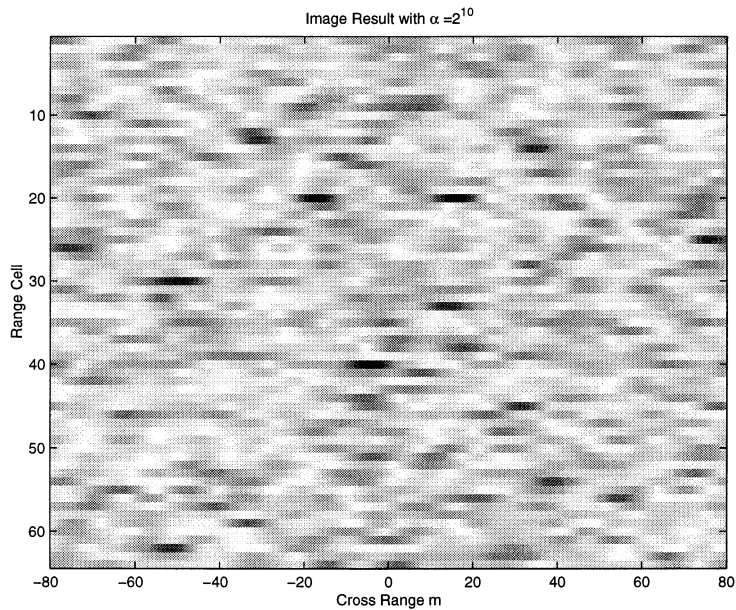
CORRESPONDENCE   657

Image Result with $\alpha = 2^{10}$

Fig. 12.   Imaging result with $\alpha = 2^{10}$.

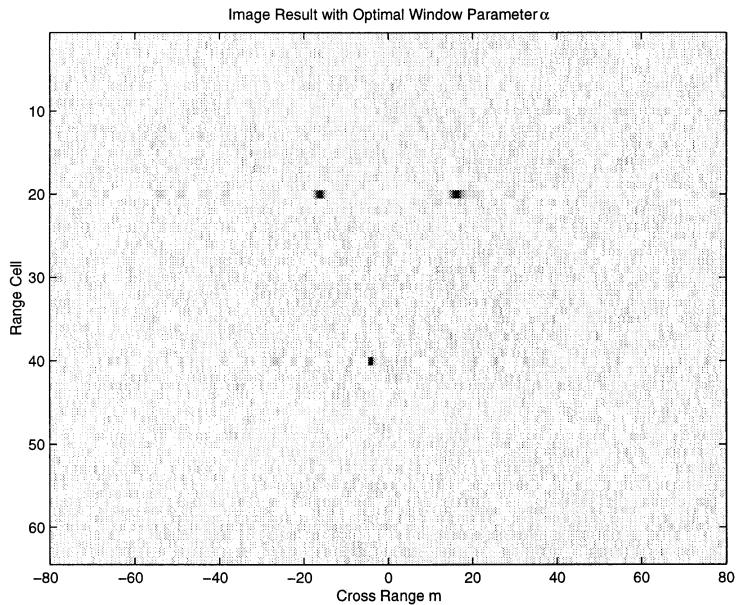Image Result with Optimal Window Parameter α

Fig. 13.   Imaging result with optimal parameter α.

and the STFT with different window parameters. In these simulations, the radar wavelength is $\lambda = 0.03$ m, pulse repetition frequency is 200 Hz, the imaging coherent integration time is $T = 6$ s. The target consists of three point scatterers, there exist two scatterers in the 20th range bin with cross axis -16 m and 16 m, respectively, and there exists a scatterer in the 40th range bin with cross axis -4 m. After motion compensation, the target can be treated as turn-table target with angle rotating velocity about $v(t) = \lambda/4\pi(8t + \frac{2}{2}t^2)$. The target rotates with a constant acceleration. The received signals of the three scatterers are: $s_1(t) = \exp(-j16(8t + \frac{2}{2}t^2))$, $s_2(t) = \exp(j16(8t + \frac{2}{2}t^2))$ and $s_3(t) = \exp(-j4(8t + \frac{2}{2}t^2))$,

respectively. The return of the 20th range bin has two linear chirp signals and white Gaussian noise with $\mathrm{SNR}_t = 0$ dB and with the same noise level in each range bin. The return of the 40th range bin is also the combination of a linear chirp signal and noise with the same target reflectivity and noise level. The rate, initial frequency, and the rate of the frequency is one fourth of those of the chirp signal in the return of the 20th range bin. So the signal in 20th rangebin is spread about 4 time more than that in 40th range bine. The image of the target by the traditional range-Doppler method is shown in Fig. 4. The images of the STFT slice with window parameters $\alpha = 2^{-2}$, 1, 2, 2^2, 2^4, 2^6, 2^8, and 2^{10} are

IEEE TRANSACTIONS ON AEROSPACE AND ELECTRONIC SYSTEMS   VOL. 38, NO. 2   APRIL 2002

shown from Figs. 5–12, respectively. We can find that the imaging quality is high in Fig. 8 and Fig. 9, where the window parameters are almost the same as the signal chirp rate, and the SNRs in Figs. 8 and 9 are higher than that in others. Fig. 13 shows the imaging result to the same data in Fig. 5 with the optimal window parameter α, i.e., the window parameter α is chosen as 2^5 in 20th range cell and α is chosen as 2^3 in 40th range cell. For more imaging results of joint TF algorithm to real data and simulation data, see [3–5].

V. CONCLUSION

In this paper, we studied the SNR increase for the ISAR image for maneuvering targets using JTFA, in particular the STFT, proposed by Chen, et al. in [1–5]. The 3 dB SNR of the STFT for LFM signals were analytically calculated. The SNR is theoretically and numerically shown better than the one using the conventional Fourier transform ISAR imaging method.

XIANG-GEN XIA
GENYUAN WANG
Dept. of Electrical and Computer Engineering
University of Delaware
Newark, DE 19716
E-mail: (xxia@ee.udel.edu)

VICTOR C. CHEN
Radar Division
Naval Research Laboratory
Washington, DC 20375

REFERENCES

[1]   Chen, V. (1994)
      Radar ambiguity function, time-varying matched filter, and optimal wavelet correlator.
      Optical Engineering, **33** (1994), 2212–2217.

[2]   Chen, V. (1995)
      Reconstruction of inverse synthetic aperture radar image using adaptive time-frequency wavelet transform.
      SPIE Proceedings, Wavelet Applications, **2491** (1995), 373–386.

[3]   Chen, V., Trintinalia, L., and Ling, H. (1996)
      Applications of JTFA to radar image processing.
      In S. Qian and D. Chen (Eds.), *Joint Time-Frequency Analysis*.
      Englewood Cliffs, NJ: Prentice-Hall, 1996, ch. 10.

[4]   Trintinalia, L., and Ling, H. (1997)
      Joint time-frequency ISAR using adaptive processing.
      IEEE Transactions on Antennas and Propagation, **45** (1997), 221–227.

[5]   Chen, V., and Qian, S. (1998)
      Joint time-frequency transform for radar range-Doppler imaging.
      IEEE Transactions on Aerospace and Electronic Systems, **34** (Apr. 1998).

[6]   Xia, X-G. (1998)
      A quantitative analysis of SNR in the short-time Fourier transform domain for multicomponent signals.
      IEEE Transactions on Signal Processing, **46** (Jan. 1998), 200–203.

[7]   Xia, X-G., and Chen, V. (1999)
      A quantitative SNR analysis for the pseudo Wigner-Ville distribution.
      IEEE Transactions on Signal Processing, **47** (Oct. 1999), 2891–2894.

[8]   Barbarossa, S., and Petrone, V. (1997)
      Analysis of polynomial-phase signals by the integrated generalized ambiguity function.
      IEEE Transactions on Signal Processing, **45** (Feb. 1997), 316–327.

[9]   Barbarossa, S. (1995)
      Analysis of multicomponent LFM signals by a combined Wigner-Hough transform.
      IEEE Transactions on Signal Processing, **43** (June 1995), 1511–1515.

[10] Boashash, B. (1991)
      Time-frequency signal analysis.
      In S. Haykin (Ed.), *Advances in Spectrum Analysis and Array Processing*, Englewood Cliffs, NJ: Prentice-Hall, 1991.

[11] Cohen, L. (1995)
      Time-Frequency Analysis.
      Englewood Cliffs, NJ: Prentice Hall, 1995.

[12] Qian, S., and Chen, D. (1996)
      Joint Time-Frequency Analysis.
      Englewood Cliffs, NJ: Prentice-Hall, 1996.

[13] Rihaczek, A. W. (1969)
      Principles of High-Resolution Radar.
      New York: McGraw-Hill, 1969.

[14] Chen, V. (1998)
      Time-frequency analysis of SAR image with ground moving targets.
      SPIE Proceedings, **3391** (Apr. 1998), 295–302.

[15] Curlander, J. C., and McDonough, R. N. (1991)
      Synthetic Aperture Radar—System and Signal Processing.
      New York: Wiley, 1991.

[16] Soumekh, M. (1999)
      Synthetic Aperture Radar Signal Processing with MATLAB Algorithms.
      New York: Wiley, 1999.

Track Association and Track Fusion with Nondeterministic Target Dynamics

Representative track fusion algorithms and track association metrics are quantitatively compared using a simple linear-Gaussian–Poisson model, under various degrees of nondeterministicitity of the target dynamics, i.e., process noises, and of the initial condition uncertainty. Track fusion algorithms are compared using an analytical method, while track association metrics are evaluated by Monte Carlo simulations.